Enhanced mechanical and biocompatibility performance of $Ti_{(1-x)}Ag_{(x)}$ coatings through intermetallic phase modification

Cecil Cherian Lukose [a], Corentin Chavignon [b], Theodora Mantso [c], Mihalis I. Panayiotidis [c,d,e], Martin Birkett [a*].

[a] Department of Mechanical and Construction Engineering, Northumbria University, Newcastle Upon Tyne, UK.

[b] ENSIAME, Université de Valenciennes et du Hainaut-Cambrésis, Le Mont-Houy 59313 Valenciennes, Cedex 9, France.

[c] Department of Applied Sciences, Northumbria University, Newcastle Upon Tyne, UK.

[d] Department of Cancer Genetics, Therapeutics & Ultrastructural Pathology and [e] Cyprus School of Molecular Medicine, The Cyprus Institute of Neurology & Genetics, Nicosia, Cyprus.

* Corresponding author, martin.birkett@northumbria.ac.uk

Abstract

Advanced materials combining superior mechanical and biocompatibility performance are of significant interest to extend the lifetime of biomedical devices. In this work, Ag is alloyed with Ti to investigate the role of emerging Ti-Ag intermetallic coatings with high mechanical hardness and exceptional biocompatibility. Thin films of $Ti_{(1-x)}Ag_{(x)}$ were deposited on 316L steel and glass substrates using magnetron sputtering and subsequently heat-treated to aid Ti-Ag intermetallic development. Mechanical properties were then measured and correlated to microstructural and morphological changes in the Ti-Ag films. In the as-grown state, the Ti-Ag matrix developed different intermetallic structures which increased the hardness of pure Ti films from 5 to >7 GPa. After heat treatment, a peak hardness of 7.39 GPa and elastic modulus of 105 GPa was achieved for a 43 at.% Ag film due to formation of the tetragonal Ti-Ag phase and increase of upper surface oxides which act as dislocation barriers. However, at higher Ag concentrations, heat treatment leads to agglomeration of Ag around grain boundaries and decreases the crystallite size, leading to reduction in hardness to <3 GPa. The Ti rich films also depict better cytotoxicity performance following exposure to the L929 cell line, though excellent cell viability values >98% are observed for the entire Ti-Ag range. While leached ion concentrations lower than 100 ppb demonstrate excellent biocompatibility of this Ti-Ag alloy system. This work demonstrates the first successful attempt to develop biocompatible Ti-Ag thin film coatings with high mechanical hardness with the potential to extend the lifetime of medical implants.

Keywords: Ti-Ag thin film coatings; hardness; biocompatible; cell viability; orthopaedic implants.

1. Introduction

Pure titanium (Ti) and its chemical forms (oxides, nitrides and alloys) showcase excellent biocompatibility, corrosion resistance and mechanical properties and have therefore been extensively used in almost all forms of orthopaedic and dental support devices [1-6]. Depending upon the area of application, these devices can play a wide variety of roles from providing temporary structural support to recovering bones [7], long term replacement of joints [8], filling dental cavities or sensing stimulus change in the implantation area [2-4]. Orthopaedic implants are increasingly used to partially support or wholly replace parts of the human skeletal system suffering problems due to increased life expectancy, various genetic defects, and increased damage from day-to-day incidents [6, 7] and are therefore expected to have superior mechanical performance to extend their lifetime under daily cyclic usage. The poor tribological performance of Ti_6Al_4V alloy, commonly used to make these implants, can also lead to the formation of fine wear debris when subjected to

continuous movement of joints. These fine debris, containing aluminium (Al) and vanadium (V), can cause toxicity to the biological systems [9] surrounding the implant while also causing premature loosening of the joint, leading to a reduction in implant life and a requirement for costly reconstruction surgery. Moreover, medical devices made from stainless steel are prone to corrosion in acidic and chloride rich environments which are common within biological systems [10]. This raises the need for careful materials selection for orthopaedic implant manufacture to ensure enhanced mechanical hardness, wear resistance and biocompatibility performance. It is critical that the biomaterials used to fabricate these implants have the right combination of mechanical, morphological, structural and biomedical properties to extend their lifetime within the human body.

Many modifications like nitriding [10-14], oxidizing [15-18] and multi element alloying [19] have been used to enhance the mechanical properties of Ti and its alloys to make them better suited for biomedical implants. Nitriding and oxidising are an efficient way of improving the mechanical properties of Ti as these interstitials increase the defect densities within the Ti matrix. However, the brittle nature of TiN coatings prepared by physical and chemical vapour deposition techniques are observed to be susceptible to delamination under load bearing conditions, while other techniques like ion implantation, result in a thinner coating surface [20]. Whereas, titanium oxide is polymorphic (anatase and rutile being the main two forms) and its biomedical and mechanical properties are heavily depended upon the processing conditions used to achieve the film microstructure [21]. Traditional TiN based coatings can be further modified into multi-element alloys by addition of a ternary or quaternary elements like Cu, Ag, Nb, Zr etc. to impart additional features like superior mechanical or anti-bacterial properties [22, 23]. Multi-element alloys like Ti-Nb-Zr-Ta-Si-Fe report high hardness values while maintaining Young's modulus values below 90 GPa, which is highly beneficial for reducing the stress shielding effect leading to poor bone recovery due to the high elastic modulus of load bearing implants [19]. However, alloying with multiple transition metals, maintained in an exact stoichiometric composition, is a complicated process to be employed in a commercial manufacturing setting for mass production of implants with longer lifespan. An alternative method to extend the life cycle of Ti-alloy based artificial joints is by coating them with a thin layer of material with superior mechanical properties. Ti-based alloys with enhanced mechanical and biomedical properties can be easily sputter deposited onto the underlying implant surface and could play a crucial role in extending their lifecycle.

Silver (Ag) and its nanostructured material system has gained much attention because of its strong antibacterial and biomedical properties [24]. Ag films have a strong tendency to agglomerate from their alloy matrix and provide a surface area to release Ag ions which inhibit the development of biofilms required for bacterial colony formation [25]. This could be particularly useful to fight bacteria during the initial stages of post-surgery recovery when the biological environment surrounding the newly implanted device is highly susceptible to infection and complications thereafter. Ag doping has also been studied extensively with other mechanically superior Ti-based material systems like TiN [26-31] and TiO [24, 32-37] to enhance their antimicrobial and bactericidal properties. Pedrosa et al. [28], explored the effect of increasing Ag atomic concentration in a TiN matrix, from 0 to 100% and observed a marked variation in open circuit potential (OCP) with grain size variation brought by addition of Ag in the TiN matrix. Yu et al. [32], found that addition of Ag in a TiO_2 matrix leads to formation suppression of the anatase phase and leads to better photocatalytic activity than baseline TiO_2. However, very few studies have been performed on alloying of elemental Ti and Ag, and work to date has focussed on the electrical and fracture resistance mechanism of these materials over a limited Ag concentration range of less than 26 at.%, for development of thin film based stretchable electrodes [2-4, 6]. Ag nanoparticles dispersed in the $Ti/TiN/TiO_2$ matrix is very well known for development of bio-electrical devices like sensors and electrodes for application within the human body, because the Ag particles can enhance conductivity without effecting the biocompatibility of the Ti alloy. Lopes et al. [2] experimented by alloying Ag with elemental Ti up to 71 at.% and found improvement in fracture resistance with addition of ductile Ag in the matrix, caused by formation of the Ti_2Ag intermetallic phase. Lopes et al. [6] also observed that annealing of Ti-Ag thin films led to enhancement of intermetallic compounds with the formation of a smoother and denser microstructure with higher grain sizes, resulting in a reduction of electrical resistivity of the alloyed thin film, but did not explore the biocompatibility of these thin films. However, recent studies show that thin film deposition of Ti alloyed with Ag can lead to enhancement of mechanical properties, with

hardness values greater than 8 GPa and Young's modulus lower than 160 GPa [3]. In the correct stoichiometry and with fine tuning of heat treatment temperature, Ti doped with transition metals like Ag, starts forming intermetallic compounds like Ti_2Ag and TiAg at Ag concentrations above 20 and 27 at.% respectively, which then exhibit superior mechanical properties [3, 4, 38]. While these studies explore mechanical or biocompatibility properties of the Ti-Ag thin films independently for a limited Ag concentration range, no previous attempts have been made to study the combined mechanical and biomedical performance of Ti-Ag thin films across all of the Ti-Ag intermetallic compounds, as done by Pedrosa et al. for Ag in a TiN matrix, while simultaneously exploring the effect of post deposition heat treatment on the development of these Ti-Ag intermetallic alloy structures.

In this work we study the effect of Ag concentration and heat treatment temperature on the formation of all known Ti-Ag intermetallic compounds and the subsequent effect of these intermetallics on the biocompatibility and mechanical performance of Ti-Ag thin film coatings deposited on biocompatible 316L stainless steel and glass substrates. The generated mechanical properties of hardness and Young's modulus are correlated with the structural, chemical, and morphological changes in the thin films, brought about by the variation in Ti-Ag composition and exposure to high temperature heat treatment. The biocompatibility of the Ti-Ag intermetallic compounds is also evaluated to confirm the retention of this feature from the individual elements in their alloy state. This work is the first attempt to compare the mechanical and biomedical performance of Ti-Ag intermetallic compounds in thin film format and explore the effect that heat treatment has on enhancing these properties to develop coating materials of high mechanical hardness for application in prolonging the life of orthopaedic implants.

2. Materials and methods

2.1 Thin film deposition:

Five compositions of $Ti_{(1-x)}Ag_{(x)}$ (x=0-1) thin films were prepared by co-sputtering 100 mm circular targets of 99.99% pure Ti and 99.999% pure Ag (supplied by Testbourne Ltd, UK), using a sequential sputtering system (Teer Coatings UDP350). Two separate targets of Ti were run simultaneously to match the high deposition rate of the single Ag target. Laboratory standard soda lime glass slides (75 x 25 x 1 mm), together with 316L stainless steel (25 x 20 x 1 mm) were used as substrates. The steel substrates were polished using SiC abrasive papers for 5 minutes each to achieve average surface roughness values better than 1 µm, before being cleaned for 2 minutes with a 1:5 ratio solution of Decon 90 detergent:water, followed by a rinse in isopropyl alcohol and blow dry with nitrogen. The centre of each glass slide was covered by high temperature Kapton tape during deposition, which was later peeled off to permit measurement of the deposited film thickness using a surface profilometer. The substrates were loaded onto a carousel inside the deposition chamber at a fixed target to substrate distance of 130 mm and rotated at a constant speed of 5 rpm. The chamber was evacuated to a base pressure better than 0.5 mPa and a working pressure of 0.3 Pa was achieved by introducing 30 sccm of Ar gas. All three targets were connected to DC power sources and pre-sputtering was carried out under closed shutters for 10 minutes to clean the target surfaces. The DC power applied to the targets was varied to achieve the five film compositions shown in Table 1, corresponding to two pure elemental Ti and Ag thin films at either extreme and three Ti-Ag intermetallic phases as per the Ti-Ag phase diagram shown in Figure 1. Following deposition, the thin films were subjected to annealing in a tube furnace (Carbolite Gero) at a temperature of 300 ˚C for 1 hour in an open air environment, to study the effect of heat treatment on the biocompatibility and mechanical hardness of the Ti-Ag films.

2.2 Thin film characterization:

The crystal structure of the coatings was analysed by X-ray diffraction (XRD) in parallel beam geometry with a Siemens D5000 X ray diffractometer using Cu-Kα radiation, in a 2θ range from 30° to 80°, measured in steps of 0.01˚ and a scan rate of 4˚/min. The results were evaluated using DiffracPlus EVA software (Bruker AXS, Karlsruhe, Germany) and compared with reference patterns from the ICSD database. The crystallite size of the structures were calculated using the Scherrer equation [39]:

$$\tau = K\lambda/\beta\cos(\theta)$$

Where τ = crystallite size in nm, k = 0.9 is the correction factor, λ = 1.5406 Å is the wavelength of the copper (Cu) X-ray source, β is the full width at the half maximum in radians and θ is the peak position angle. Surface imaging was performed using a Tescan MIRA 3 scanning electron microscope (SEM) system and compositional information was collected using a built in Oxford instruments X-Max 150 energy dispersive X-ray spectroscopy detector. Nanoindentation was performed using a Hysitron TI900 system with a 3-sided Berkovich tip with half angle of 65.27°. Hardness and elastic modulus were measured over a 10-10-10 second load-dwell-unload cycle and the unloading leg of the force displacement curve achieved from the Oliver and Pharr indentation technique [40]. For each sample, a 4x4 indentation pattern with a 5 µm indent interval was made, up to a total indentation depth of 10% of the film thickness by varying the peak load from 1 to 0.7 mN. The surface roughness of the deposited films was measured using a Nanoveeco Dimension 3000 AFM in contact mode using a 15 nm silicon tip. The thickness of the as-grown and heat-treated films was measured using a Dektak XT stylus profilometer across the step height created by removal of the Kapton tape from the glass slides.

2.3 Biocompatibility characterization:

The biocompatibility study was performed in accordance with the ISO 10993 standard using the Alamar blue assay to evaluate the cytotoxicity of the Ti-Au films. Dulbecco's Modified Eagle Medium (DMEM), phosphate buffer saline (PBS), Fetal Bovine Serum (FBS), trypsin, penicillin/streptomycin and L-glutamine were obtained from Labtech International Ltd (Sussex, UK). The murine fibroblast (L929) cell line and resazurin sodium salt were purchased from Sigma-Aldrich (St. Louis, MO, USA). All chemicals were of analytical grade and obtained from Invitrogen (Carlsbad, CA, USA), Applichem (Darmstadt, Germany) and Sigma-Aldrich. The L929 cell line was maintained in low glucose DMEM supplemented with 10% FBS, 2 mM L-glutamine and 1% pen/strep (100 U/ml penicillin, 100 µg/ml streptomycin). Cells were cultured for 15-20 passages in a humidified atmosphere at 37°C and 5% CO_2, grown as monolayers and sub-cultured at 80-90% confluency. The Ti-Ag thin film test samples were disinfected in 70% ethanol solution and left to air-dry before being transferred into sterile tubes containing complete medium (15 ml). They were vortexed, at low speed, for 5 secs and then incubated at 37°C for 72 hours to allow the samples to leach. At the end of the incubation period, samples were again vortexed, at low speed, for 5 secs and each sample was removed from the medium solution which was eventually used for treating cells. A polished piece of Cu (25x20x1 mm) was used as a positive cytotoxic control (i.e. control introducing positive cytotoxic effects to the L292 cells) and extracts were prepared under the same conditions as the Ti-Ag thin film samples. L929 cells (2,000 cells/well) were seeded into 96-well plates in 100 µl/well and incubated for 24 hours prior to exposure to the extracts from the test samples and positive control. On the following day, cells were exposed to two dilutions (50 and 100% (v/v)) of extracts for 72 hours. For negative cytotoxic control conditions (i.e., controls introducing no cytotoxic effect towards L929 cells), cells were incubated with complete medium only, while medium containing 10% Dimethyl Sulfoxide Solution (DMSO) was used as a second positive cytotoxic control (i.e. at this concentration DMSO is cytotoxic to any cell line). After 72 hours, fresh medium (containing 0.1 mg/ml resazurin) was added into each well and incubated for 2 hours at 37°C while the Alamar-blue assay was utilized for the determination of cell viability. The assay uses blue-coloured resazurin which is converted to purple-coloured resorufin, in metabolically active cells, with the resulting increase in absorbance being proportional to the levels of viable cells. The plates were then centrifuged and absorbance was recorded at 570 nm and 600 nm (reference wavelength) using a Spark multimode plate reader (Tecan, Switzerland). Levels of cell viability were measured and expressed as percentage of control cells. Finally, the extracts prepared from the Ti-Ag films and Cu positive control samples were tested in a Perkin Elmer Optima 8000 inductively coupled plasma optical emission mass spectrometer (ICP-OEMS) to quantify levels of ions released in each extract after 72 hours of incubation. Standards were prepared (for a range of 1, 5 and 10 ppm) to measure levels of dissolved Ti, Al, V, Cu and Ag leached from the Ti-Ag films and positive Cu control sample.

3. Results and discussion

3.1 Chemical and morphological characterization:

Elemental composition and film thickness of the five Ti-Ag thin film samples are shown in Table 1. EDX measurement was made across 5 sites on each thin film surface and values averaged, with standard deviation better than 0.9 at.% in each case. Film thickness was measured across 4 locations on the film-glass step and averaged, with thickness variation less than ±10 nm for all samples. The average thickness of the as-grown films shows an increasing trend from 642 nm to 710 nm with increase in Ag concentration in the films due to the higher deposition rate of Ag when compared to Ti [41]. The five thin film samples cover the whole Ti-Ag composition range, starting with pure Ti (S_0) and thereafter one composition for each of the three main regions of the Ti-Ag phase diagram ($S_{0.24}$, $S_{0.43}$ and $S_{0.59}$) as shown in Figure 1, and lastly a pure Ag film (S_1). After heat treatment at 300°C for 1 hour in open air, the thickness for these films increases to 700+ nm with a 6-18% increment in thickness with increasing Ag content in the films. EDX results following heat treatment show higher oxygen concentration levels between 18.2-22.6 at.% for the films containing Ti when compared to the pure Ag film, which shows only 6.8 at.% oxygen. Ti and its alloys are well known for their high reactivity, and annealing in open air environment at high temperature will lead to inclusion of oxygen within the Ti-Ag matrix [42-48].

Table 1: Film thickness and elemental composition of $Ti_{(1-x)}Ag_{(x)}$ films as-grown and after heat treatment.

Sample ID	Power (W)		As-Grown			Heat-Treated			
	Ti	Ag	Average thickness (nm)	Average composition (at.%) [std. dev] Ti	Ag	Average thickness (nm) [increase after heat treatment]	Average composition (at.%) Ti	Ag	O
S_0	640	0	642	100.0	00.0	705 [+63]	81.5[0.42]	00.0	18.5[0.42]
$S_{0.24}$	541	26	685	75.9[0.12]	24.1[0.12]	778 [+93]	61.5[0.48]	20.8[0.38]	18.2[0.19]
$S_{0.43}$	374	38	661	56.9[0.36]	43.1[0.36]	700 [+39]	44.5[0.30]	33.3[0.40]	22.6[0.23]
$S_{0.59}$	254	52	638	41.0[0.20]	59.0[0.20]	757 [+119]	32.8[0.56]	47.4[0.63]	19.8[0.90]
S_1	0	104	710	00.0	100.0	785 [+75]	00.0	93.8[0.48]	06.8[0.48]

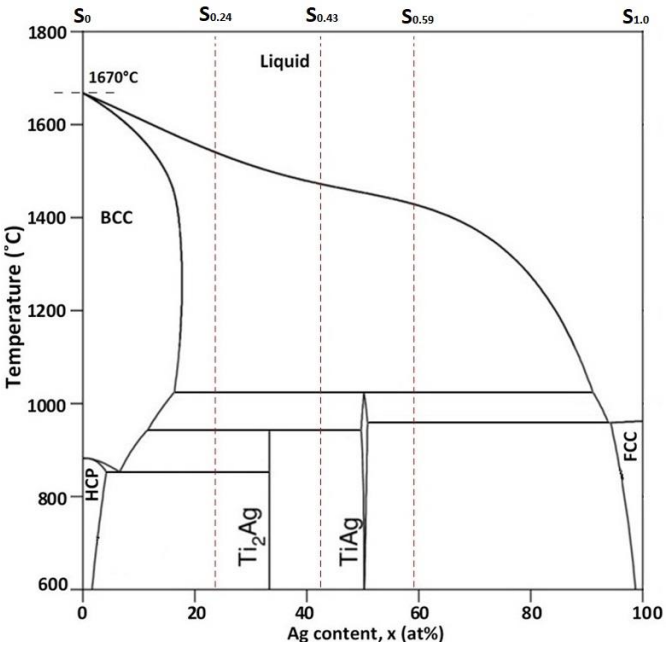

Figure 1: Phase diagram of the Ti-Ag system showing the Ag concentration of the deposited Ti-Ag thin films and their respective Ti-Ag intermetallic regions [49].

3.2 Structural characterization:

The structural characterization for the Ti-Ag films deposited on glass substrates was performed by XRD and the developed diffraction patterns for each thin film composition in its as-grown and heat-treated state are shown in Figure 2 (a)-(e). The as-grown pure Ti thin film (S_0) exhibits a hexagonal closed packed structure with the highest peak intensity at 38.4°, representing the preferred orientation along (002) of the α-Ti phase [2]. However, after heat treatment at 300°C, the peak for the (011) orientation at 40.2° becomes dominant in this phase. Higher heat treatment temperature favours the enhanced mobility of adatoms on the film surface and leads to increased intensity of the (011) direction [50] for this sample. With the addition of Ag, sample $S_{0.24}$ exhibits a very sharp peak of high intensity at 38.2° indicating the formation of the Ti_2Ag (113) intermetallic phase. Indexing of the Ti-Ag intermetallics (Ti [ICSD no. 43416], Ti_2Ag [ICSD no. 605931], TiAg [ICSD no. 58369] and Ag [ICSD no. 53759]) is very difficult because of their close angular peak positions and if the preferred orientation overlaps then the diffraction pattern can be assigned to intermixing of the phases suggested by the Ti-Ag phase diagram [3]. The Ti-Ag phase diagram favours the formation of the Ti_2Ag intermetallic phase for $S_{0.24}$. The smaller peaks at 35.4˚ and 40.2˚ suggest coexistence of metallic HCP α-Ti together with the intermetallic Ti_2Ag phase in the film. Further increments of Ag concentration in $S_{0.43}$ and $S_{0.59}$ leads to formation of the tetragonal TiAg (011) intermetallic phase with a sharp (011) reflection at 37.9°. No additional metallic Ti peaks are visible for these Ag concentrations which, according to the Ti-Ag phase diagram, favours the solid solution of TiAg and Ti_2Ag intermetallic phases. For all the intermediate Ti-Ag compositions ($S_{0.24}$, $S_{0.43}$, $S_{0.59}$), a small peak at 81.1° could be observed and can be matched to the Ag (222) phase in the reference patterns. Ag is known for cluster formation when deposited with Ti, agglomerating at the grain boundaries [44, 51]. Therefore, the presence of the metallic Ag peak is expected, especially at higher Ag concentrations. Finally for the pure Ag thin film (S_1) the result matches the diffraction pattern and shows a face centred cubic structure and predominant peak position at 38.2°, representing the (111) orientation of crystallites [52, 53]. Heat treatment of the Ti-Ag films in open air leads to oxidation of the film surface (as shown in Table 1) but no crystalline peaks corresponding to the oxides of Ti or Ag are visible in the XRD patterns in Figure 2. Ti oxides are amorphous and only crystallizes when heat-treated above 400°C. However, an increasing concentration of Ag in the film pushes the crystallization temperature of the TiO_2 anatase phase to higher temperatures [44]. Therefore, no crystalline oxide phases of TiO_2 are observed in the XRD results.

Figure 2 (f) shows the variation in the average crystallite size with increasing Ag content in the Ti-Ag thin films before and after heat treatment. The as-gown films show an increment of crystallite size from 17 to 45 nm for S_0, $S_{0.24}$, $S_{0.43}$, $S_{0.59}$ and S_1 respectively. The unusual decrease in the crystallite size for $S_{0.43}$ can be explained by the increased agglomeration of Ag atoms (shown in the SEM images in Fig 4) at this composition and the emergence of multiple phases of tetragonal Ti_2Ag and TiAg intermetallic structures [3, 4]. Figure 2 (a and e) clearly show that heat treatment enhances the crystallinity of the pure Ti (S_0) and pure Ag (S_1) films and the resulting increment in crystallite size for these films is clearly visible in Figure 2 (f) and can be related to annealing of structural defects. Sample $S_{0.24}$ registers an increase in the average crystallite size from 22 to 25 nm following heat treatment. The increase in thermal energy from the heat treatment will lead to an increase in the agglomeration of Ag and this leads to rearrangement of the multiple phases of the intermetallic structure formed (TiAg or Ti_2Ag) in the crystal, thereby reducing the crystallite size of the final intermetallic compound [3, 4]. But this reduction in the crystallite size of the Ti_2Ag phase is counteracted by the increase in size in the Ti phase and therefore, registers a slight increase in overall crystallite size. On the other hand, $S_{0.43}$ and $S_{0.59}$ show a decrease from 19 and 24 nm to 18 and 22 nm, respectively, due to segregation of the TiAg and Ti_2Ag phase rearrangement.

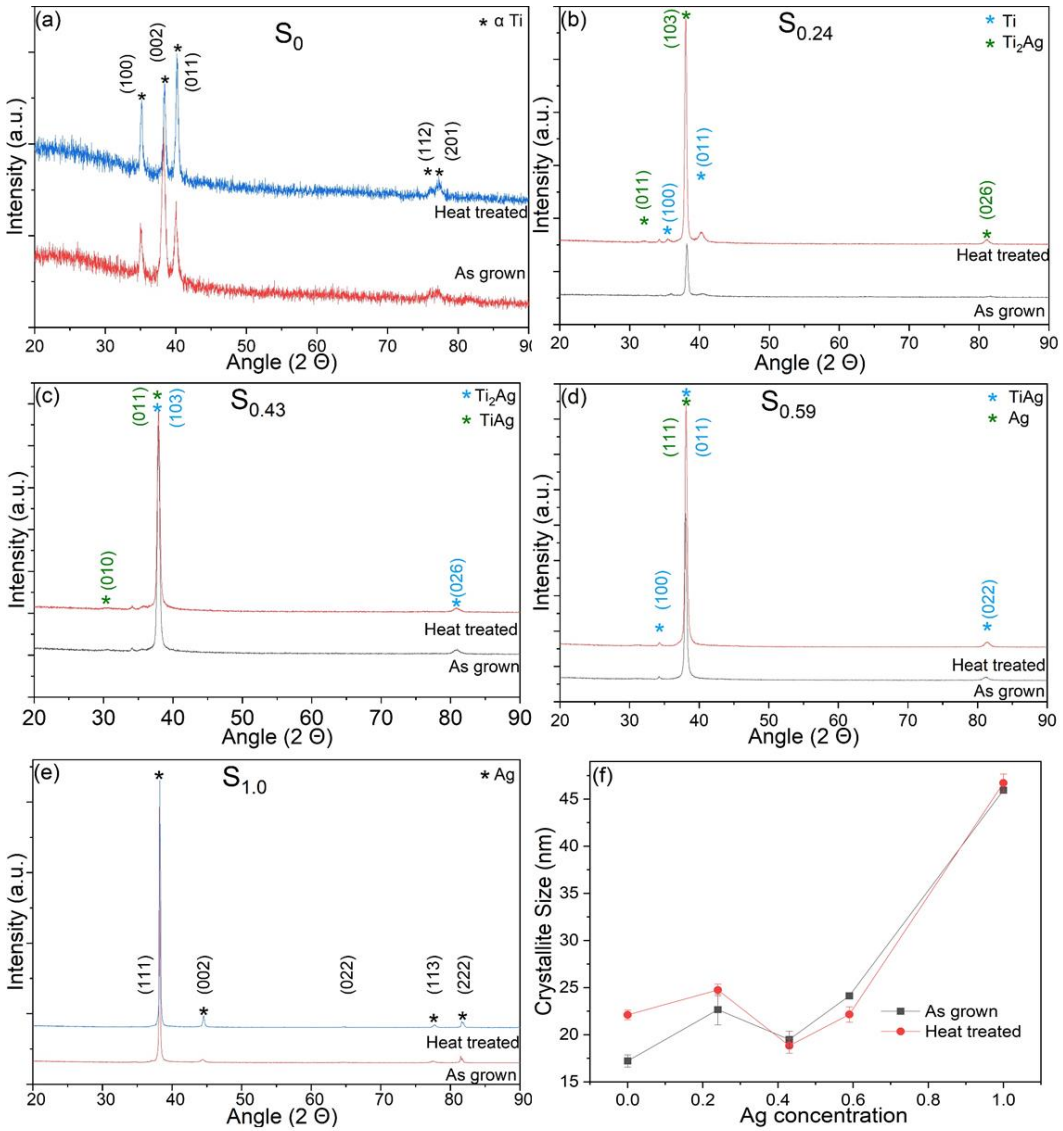

Figure 2: (a-e) XRD patterns for $Ti_{(1-x)}Ag_{(x)}$ films with increasing Ag concentration in film. (f) Calculated crystallite sizes for $Ti_{(1-x)}Ag_{(x)}$ films as-grown and heat-treated.

Surface morphology of the as-grown and heat-treated Ti-Ag films is shown in Figure 3 (a-e) and (f-j), respectively. The as-grown Ti film (Fig 3a) forms large triangle shaped grains but addition of Ag in the film ($S_{0.24}$-Fig 3b), leads to formation of fine dome shaped Ti-Ag grains. Though with further increment of Ag concentration to 43 at.% (Fib 3c), the grains become much finer, however, visible particles of pure Ag are seen distributed across the film surface because of the increased rate of Ag agglomeration. However, with further addition of Ag, for sample $S_{0.59}$ (Fig 3d) the agglomeration subsides as the Ag phase begins to dominate, marked by the appearance of well defined, dome-shaped grains. While for the pure Ag film (Fig 3e), the grains grow further and retain their dome shape. With heat treatment, the as-grown Ti film (Fig 3f) loses its well-defined shape as neighbouring grains begin to combine and form a continuous layer. Films with increasing Ag concentration ($S_{0.24}$, $_{0.43, 0.59,}$ and $_1$), show agglomeration of Ag as smaller granules coalesce to form larger granules, visible as white particles in Figure 3b, c, g and h. This result is supportive of the XRD patterns in explaining the reduction of crystallite size of the Ti-Ag intermetallic due to Ag agglomeration at higher Ag concentration and with heat treatment temperature. In Figure 3(i), the $S_{0.59}$ film shows a change from dome shape grains to a pillar like structure. The pure Ag film (Fig 3j) also loses its well-defined dome shape following heat treatment as the surface grains begin to merge.

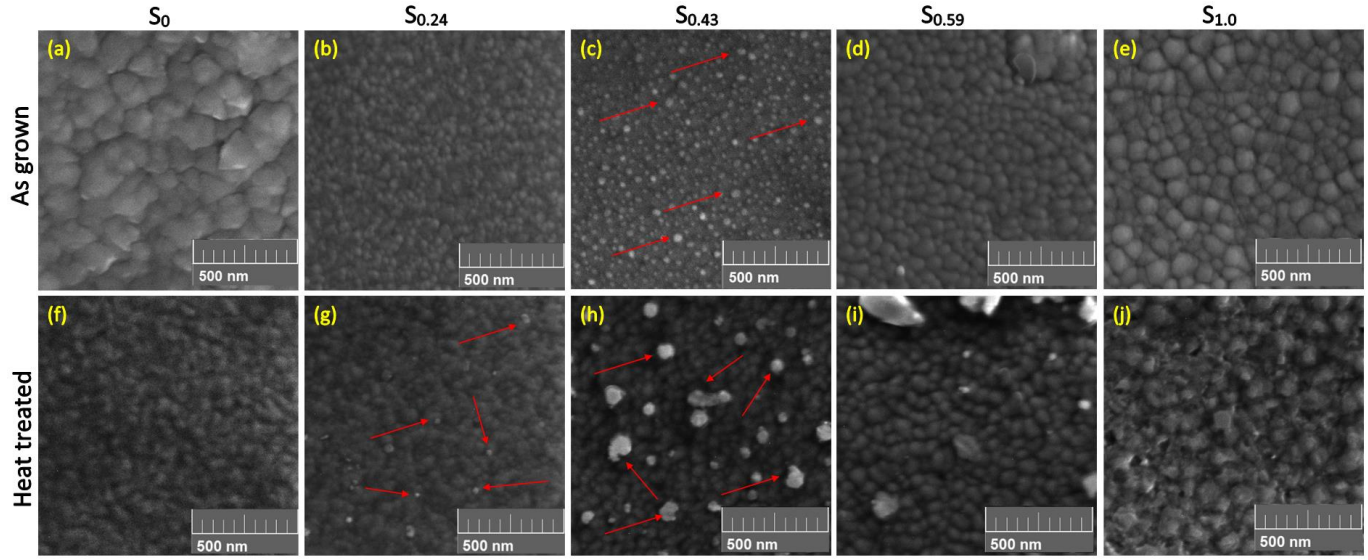

Figure 3: Surface SEM images of (a-e) as-grown $Ti_{(1-x)}Ag_{(x)}$ films in increasing concentration of Ag in the film, and (f-j) their heat-treated counterparts. (Red arrows highlight the sites of Ag agglomeration).

Cross section images of as-grown and heat-treated Ti-Ag thin film samples S_0, $S_{0.43}$ and $S_{1.0}$, are shown in Figure 4 (a-c) and (d-f) respectively. These samples are chosen to compare the cross-sectional microstructure of the Ti-Ag films with the highest hardness (as explained in section 3.4) against pure Ti and Ag thin film samples. The side profile of triangular features is visible in the cross section of the pure Ti thin film (Fig 4a) , similar to those seen on the surface images earlier with a dense glass like microstructure. After heat treatment the side profile appears smooth (Fig 4d) as though the grains have fused together, suggestive of surface oxidation, while the columnar structure becomes better defined, indicative of improved crystallization. For films with intermediate Ag concentration, small spherical structures can be seen uniformly distributed across the microstructure of sample $S_{0.43}$ (highlighted by red arrows in Fig 4b). Multiple studies have observed similar agglomeration of Ag at higher concentrations or after thermal treatment at elevated temperature [44, 51]. After heat treatment, the $S_{0.43}$ film shows the presence of faint columnar structures (Fig 4e), supporting the development of intermetallic compounds, which for this sample is known to be a mixture of TiAg and Ti_2Ag. Several larger but less frequent Ag globules (highlighted by blue arrows in Fig 4e) are formed by merging of the more uniformly spread smaller Ag granules observed in the as-grown state, suggesting that agglomeration increases with heat treatment at higher temperature. On the other hand, the pure Ag thin film shows a tapered rod like microstructure in the as-grown state (Fig 4c), which transforms to a dense glass like arrangement after heat treatment (Fig 4f).

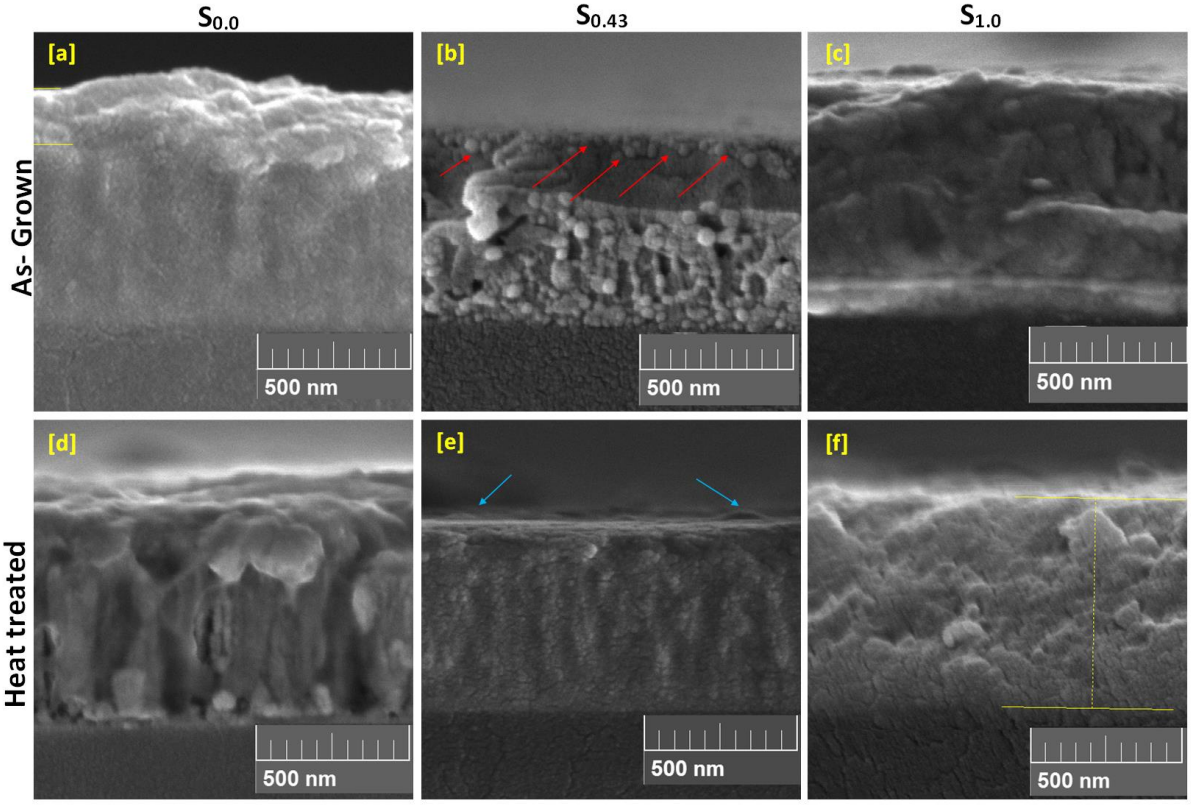

Figure 4: Cross section SEM images of (a-c) as-grown Ti(1-x)Ag(x) (x= 0, 0.43 and 1.0) films in increasing concentration of Ag in the film, and (d-f) their heat-treated counterparts.

3.3 Surface characterization:

Atomic force microscopy surface images of the Ti-Ag thin films, together with their average surface roughness values are shown in Figure 5 and 6 respectively. The well-defined hexagonal structure of the as-grown S_0 sample (Fig 5a) can be seen to reach a feature height range of 44 nm and this abruptly changes to a very fine needle shaped structure shorter than 21 nm with addition of Ag in $S_{0.24}$ (Fig 5b). The film topography remains below 20 nm for $S_{0.43}$ (Fig 5c) and then the structure begins to grow in height with further increase of Ag in $S_{0.59}$ to heights of 27 nm (Fig 5d). Thereafter the shape changes to a sharp hill like structure with significant increase in height (around 60 nm) seen for the pure Ag thin film S_1 (Fig 5e). This is also evident in the average surface roughness value which reduces with the initial addition of Ag in the Ti matrix, from 3.1 nm for S_0 to 2.3 nm for $S_{0.24}$, but with further addition of Ag in the film it begins to increase, reaching a maximum of 3.4 nm for S_1 (Fig 6). With heat treatment the surface of the pure Ti film (S_0) becomes smoother (Fig 5f) compared to the as-grown structure (Fig 5a), reducing to a surface roughness value of 2.9 nm, as the increased temperature aids recrystallization and void and defect healing between the column boundaries, resulting in a more dense and uniform structure [3, 54]. Higher oxygen concentration seen for the pure Ti and Ti-Ag thin films (see Table 1) also leads to suppression of surface features and a more uniform appearance [55]. However, for the rest of the heat-treated samples, the surface roughness shows an increasing trend with increase in Ag concentration when compared to the results for the as-grown samples (Fig 6), which is promoted by higher agglomeration of Ag particles precipitating out of the Ti-Ag matrix at higher heat treatment temperatures.

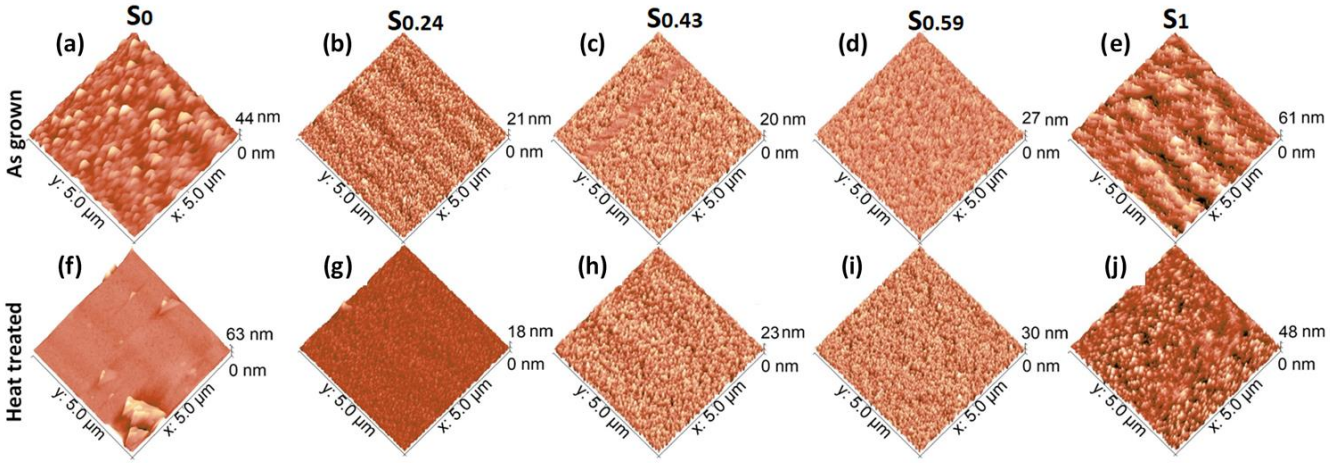

Figure 5: AFM images of (a-e) as-grown Ti-Ag thin films, and (f-j) their heat-treated counterparts.

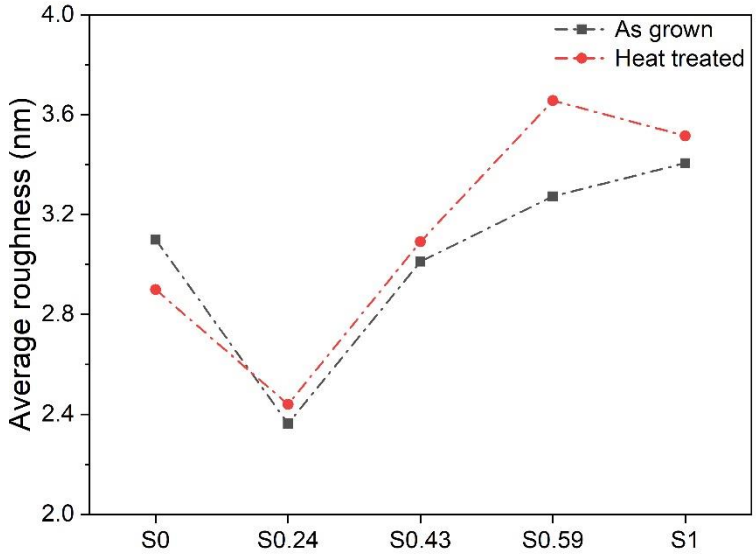

Figure 6: Average roughness variation for Ti-Ag thin films as-grown and heat-treated at 300°C.

3.4 Mechanical characterization:

In order to visualise the effect of Ag concentration and heat treatment on mechanical properties, load-displacement (P-H) curves from nanoindentation tests performed on Ti-Ag film samples S_0 and $S_{0.43}$ deposited on glass substrates, in the as-grown and heat-treated states, are presented in Figure 7. For direct comparison, each selected curve represents the indenter progress into the material when an indentation is made with a peak load of 815 µN. The loading and unloading sections for each curve do not show the presence of any “stair step” type of disruption which implies the absence of any displacement excursions or “staircase phenomena” [56, 57]. Such staircase type disruption generally occurs when the indenter encounters surface contamination, a phase transition or an oxide breakthrough event during the indentation progress [58]. However, if the discontinuities or oxide layer do not separate from the underlying layer, when under load, the tip of the indenter will continue to be supported and thereby prevent any sudden acceleration of the tip into the film, which in turn will result in smooth and staircase free load-displacement curves [59].

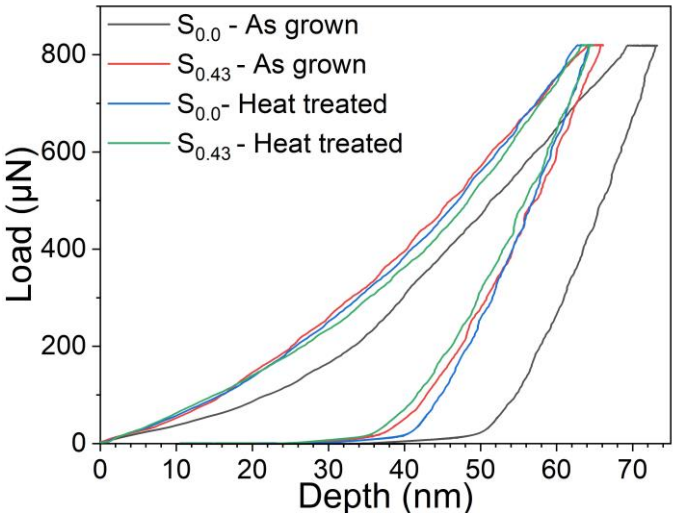

Figure 7: Load-displacement curves for the Ti-Ag thin film samples (x= 0 and 0.43), comparing the shape of the curve as-grown and after heat treatment.

Indents performed on the as-grown pure Ti thin film (black curve in Fig 7) clearly show the softer nature of this film, with the penetration depth reaching a maximum value greater than 70 nm and a calculated contact depth of 60.5 nm. This translates to a reduced elastic modulus of 105 GPa and a mechanical hardness of 4.8 GPa when its unloading segment is analysed. However, with addition of Ag, sample $S_{0.43}$ (red curve), presents greater resistance to tip penetration, registering a contact depth of 50.3 nm, resulting in increased mechanical hardness of 6.9 GPa and elastic modulus of 103 GPa. After heat treatment, the pure Ti thin film (blue curve) depicts a great improvement in mechanical performance with contact depth reducing to 50.8 nm, translating to a mechanical hardness of 6.7 GPa and an elastic modulus value of 116 GPa. Sample, $S_{0.43}$ registers only a slight improvement in mechanical performance after heat treatment (green curve), with a lower contact depth of 49.1 nm accounting for a mechanical hardness of 7.3 GPa and elastic modulus of 105 GPa. The area covered by the P-H curve indicates the work done when the indenter tip loads, dwells and unloads during the indentation process and takes into account the energy spent due to plastic deformation of the thin film [60, 61]. Heat treatment of thin films leads to better crystallization of intermetallic compounds which will lead to reduction in this mechanical hysteresis caused by plastic deformation, thereby making the films stiffer and harder [61]. While the P-H curve gives a snapshot of the mechanical performance for one sample, analysing the mean values of mechanical hardness and elastic modulus for the Ti-Ag series will help to better understand the role of Ag concentration and heat treatment in defining the mechanical performance of these thin films.

Figure 8 (a to d) compares the values of mechanical properties of reduced elastic modulus (Er) and Hardness (H) extracted from the Ti-Ag thin films in the as-grown and heat-treated states on glass and steel substrates by performing load control nanoindentation using a Berkovich tip. It can be seen that, on glass substrates, the elastic modulus of the as-grown Ti-Ag thin films steadily decreases from 110 GPa for pure Ti thin films (S_1) to 96 GPa for pure Ag thin films (S_0), with an exception for $S_{0.43}$ where it shows a very small increment in elastic modulus compared to film compositions on either side of it. The Ti-Ag films deposited on 316L steel substrates show higher values for reduced elastic modulus compared to their glass counterparts for samples $S_{0.43}$ and $S_{0.59}$ but for the rest of the films the value remains almost identical. With heat treatment of these films there is a nominal increment in the elastic modulus to 115 GPa for pure Ti thin films (S_0), which then steadily decreases to 95 GPa for pure Ag thin films (S_1), with an exception made this time by the $S_{0.59}$ sample where it increases in value compared to the film compositions on either side of it. Therefore, it can be said that heat treatment has minimal effect on elastic modulus. The size of the error bar around the mean value is seen to be larger for measurements taken from thin films deposited on steel substrates compared to those on glass. This increment in scatter arises from the increased surface roughness of the steel substrate (< 1μm) compared to glass, which has a surface roughness of around 2 nm [62-65]. Although the increased surface roughness of the steel substrates leads to a greater variation

in results when compared to those on smoother glass slides, the average hardness values recorded for each of the thin film samples are within a comparable range.

The as-grown hardness value of 5.2 GPa for the pure Ti thin film (S_1) increases with addition of Ag in the Ti matrix, reaching a peak value of 7.18 GPa for a Ag concentration of 43 at.% ($S_{0.43}$). Thereafter, the increment of Ag concentration leads to drastic reduction of hardness value, reaching the lowest point of 2.4 GPa for pure Ag (S_1). A similar trend is also observed for the hardness of these films deposited on steel substrates starting at 5.79 GPa for pure Ti thin films (S_0) and reaching a peak value of 7.06 GPa for a Ag concentration of 43 at.% ($S_{0.43}$) and thereafter reducing drastically to 2.12 GPa for the pure Ag thin film (S_1). The as-grown Ti-Ag thin films deposited on steel and glass both show an enhancement in mechanical hardness with varying Ag composition in the matrix. The pure Ti thin films are softer in nature but the Ti-Ag matrix formed by addition of Ag has irregularities and defects and the concentration of these defects dispersed within the matrix directly influences the mechanical properties. With addition of Ag, multiple Ti-Ag intermetallic phases emerge and act as barriers or pinning locations to the movement of dislocation waves from external deforming loads, like the force from the nanoindentation tip. With further addition of Ag, precipitation of Ag starts to take place at the grain boundaries, as seen from the SEM images (Fig 3) and the presence of Ag peaks in the XRD spectrums (Fig 2), which further inhibit the movement of dislocations, resulting in the improved hardness seen for the $S_{0.43}$ thin film. However, beyond the Ag concentration of 0.43 at.%, the grain size is seen to increase drastically, as seen from SEM images, leading to reduction of grain boundaries in the Ti-Ag intermetallic. This phenomenon reduces the resistance to dislocation movement in the resulting Ti-Ag matrix, which then results in a reduction in hardness of the film. Ag rich films have mechanical properties progressively similar to the pure Ag film because of the dominance of Ag rich intermetallic phases like Ti-Ag and Ag.

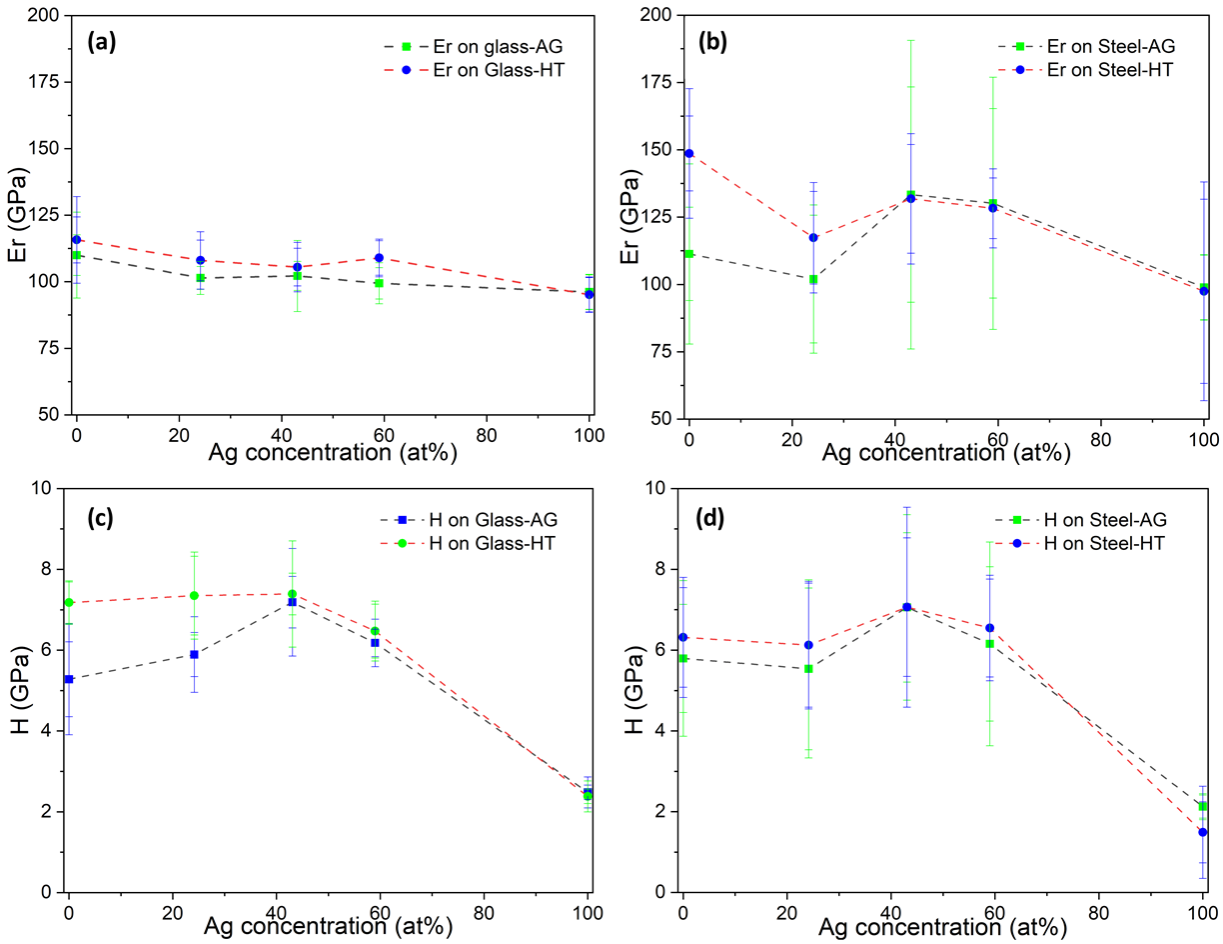

Figure 8: (a-b) Reduced elastic modulus, Er (GPa) and (c-d) Hardness, H (GPa) of as-grown and heat-treated Ti-Ag thin films deposited on glass and steel substrates.

Following heat treatment, a visible improvement in hardness is only observed for Ti rich films, which plateaus to a value of around 7 GPa for S_0, $S_{0.24}$ and $S_{0.43}$ and again the peak value of hardness is achieved for $S_{0.43}$ at 7.39 GPa. Thereafter, the heat-treatment process has no significant effect on the hardness of the Ag rich films. Thin films on steel substrates also achieve the peak hardness value of 7.05 GPa for the same Ti-Ag composition of $S_{0.43}$. After heat treatment the Ti-Ag thin films experience grain growth, defect healing, phase emergence and surface oxidation depending upon the Ag concentration. Pure Ti thin films (S_0) undergo a higher rate of oxidation and experience larger growth in grain size when compared to the other film compositions, as evident from the elemental composition analysis presented in Table 1. Grain growth is known to negatively affect hardness as it leads to a reduction in grain boundaries and therefore less resistance to any dislocation movement, but on the other hand, inclusion of titanium oxides in the film matrix is known to increase hardness as it acts as a hindrance to dislocation wave propagation [66]. Therefore, a competing effect between these two factors could explain the increment in hardness of the pure Ti thin films, which undergo heavy oxidation following heat treatment, despite the observed increase in grain size. For Ti-Ag intermetallics, the increased temperature from heat treatment leads to further agglomeration of Ag particles at the grain boundaries and oxidation, which increases hardness, while increased grain size counteracts this increment. Ag has lower reactivity towards oxygen when compared to Ti and therefore increasing the concentration of Ag in the film results in less oxides dispersed throughout the structure post heat treatment. This joint effect of oxidation and grain growth reaches a peak for a Ag concentration of 43 at.%, resulting in the maximum observed hardness value of 7.39 GPa on glass (or 7.05 GPa on steel) for this composition ($S_{0.43}$). Thereafter, for the Ag rich films, the grain size is seen to rise very steeply and causes a significant reduction in hardness which cannot be counteracted by the reduced level of oxidation taking place in the Ag rich thin film samples.

3.5 Biocompatibility characterization:

The biocompatibility test was performed using the Alamar blue assay evaluating the cytotoxicity effect of the Ti-Ag thin films on mouse fibroblast (L929) cells. Figure 9 shows the percentage of live cells (cell viability) after exposure to 100% concentration of thin film extracts for 72 hours. A solution of DMEM medium has served as a negative cytotoxic control as indicated by the observed 99.9±1.2% cell viability levels, as opposed to cells exposed to a positive cytotoxic control of 10% DMSO solution where less than 10.9±0.5% of cell viability was achieved, indicating that none of the cells were viable after such exposure conditions. On the other hand, a Cu sample (of the same dimensions as the Ti-Ag thin film samples) was used as second cytotoxic positive control in order to determine the effect of a solid substrate on cell viability. It was shown that the extract from this Cu substrate was cytotoxic with a cell viability figure lower than 1.2±0.3%. To this end, the Cu ion level released into the solution, measured using ICPOEMS, was observed to be 112 ppm and linking this with the above-mentioned reduced cell viability levels, shows that the cells are prone to toxicity effects from the ions leached in the solution if they are not biocompatible. In comparison, to the controls, the as-grown Ti-Ag thin films were shown to be highly biocompatible with cell viability levels greater than 98.88%, throughout the entire composition range, suggesting no cytotoxicity effect on the proliferation of L929 cells. Some samples are seen to register cell viability levels higher than 100% compared to the control. Such over proliferation of cells in these samples are statistically non-significant and suggest a small degree of an overestimation effect [67, 68]. Heat treatment of the Ti-Ag films at 300°C gives a slight improvement in the cell viability levels of the pure Ti (S_0) and Ti-rich ($S_{0.24}$) samples and leads to a slight reduction for the pure Ag (S_1) and Ag-rich ($S_{0.59}$) films. Our data is in agreement with previous research linking an increase in biocompatibility with an increase in crystallite size [69] and is supported by the change in average crystallite size measurements of the Ti-Ag films reported in Figure 2 (f). Overall, our data provides a clear indication that the Ti-Ag-based thin films are highly biocompatible in both as-grown and heat-treated conditions with cell viability levels being in line with those previously reported for pure Ti and Ag films [70].

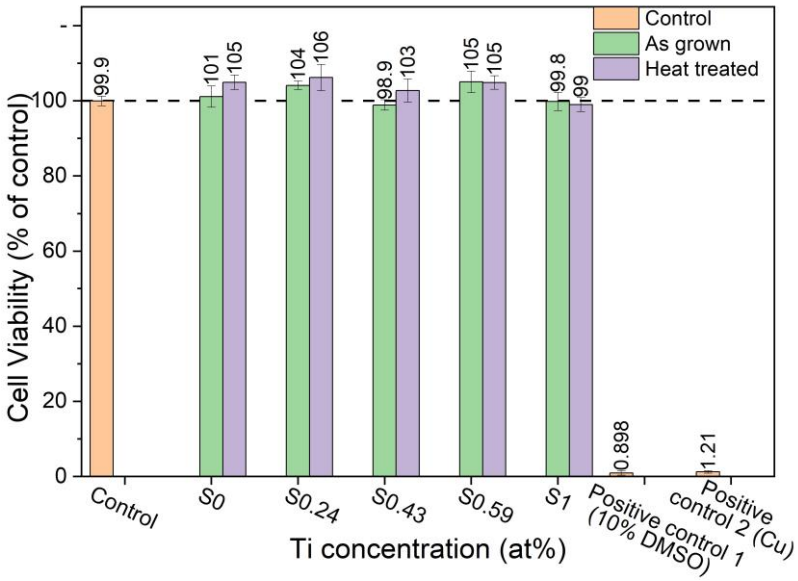

Figure 9: Bar chart showing the cell viability levels of L929 cells exposed to different concentrations of $Ti_{(1-x)}Ag_{(x)}$ thin films under as-grown and heat-treated (at 300°C) experimental conditions.

3.6 Ion release analysis:

The ICP-OEMS test performed on the Ti-Ag thin film samples and the Cu positive cytotoxic control reveals the level of Ti, Ag, and Cu ions leached into the extracts after 72 hours. These values help to understand the potential cytotoxicity effect of the material system and the effectiveness of these thin films as biocompatible coatings. Overall levels of ion concentrations observed in the extracts were 5 times lower than the detection limit of the 1 ppm standard. The highest concentration for Ti was observed for sample S_1 at 0.29 ppm. These ion concentration limits are much lower than the maximum safe concentration level (10 ppm) of Ag for human cells, while still being above the 0.1 ppb level at which Ag ions are considered to be antibacterial [71]. Such low leached Ag ion concentrations, even from the pure Ag thin film sample $S_{1.0}$, is not surprising, as previous works have observed extremely low Ag ion concentrations in the range of 5.2 ppb (0.0052 ppm) from pure Ag thin films [72] and this enables Ag based biomedical devices to remain noncytotoxic to host cells. In contrast, the extract from the Cu positive cytotoxic control prepared under the same conditions, had a Cu ion concentration of 112 ppm and was therefore found to be extremely cytotoxic to the L929 mouse fibroblast cells. Therefore, it can be said that 72 hours of exposure to DMEM medium does not cause any toxic leaching of Ti or Ag ions into the extract medium and this is reflected in the excellent cell viability values observed in Figure 9 for all Ti-Ag thin films. Recent works on Ti-Cu-Ag based materials have clearly demonstrated that Ag and Cu can enhance the mechanical properties of Ti based alloys, while also providing excellent biocompatibility. Many previous works have shown that Ag and Cu ions can be tolerated by human cells in smaller concentration, while still offering effective antimicrobial performance to reduce bacterial colony formation, because the mode of interaction between these ions and bacterial cells differ significantly from advanced mammalian cells [73-75].

4. Conclusion

Through investigation of $Ti_{(1-x)}Ag_{(x)}$ thin films deposited on 316L stainless steel and glass substrates in their as-grown and post 300°C heat treatment state, this work has successfully shown that the morphological, microstructural and chemical changes occurring in the films have a strong influence on their mechanical properties. With increasing Ag concentration, the Ti-Ag intermetallic develops and leads to an improvement in the mechanical hardness of the films. This increased hardness is caused by agglomeration of Ag at the grain boundaries leading to reduction in the crystallite size, which increases at higher temperature during heat treatment leading to further reduction in the cell size. A peak value of mechanical hardness of 7.39 GPa and relatively low value of reduced elastic modulus of 105 GPa was achieved for a Ti-Ag thin film with a Ag concentration of 43 at.%. The Ti-Ag thin films remained highly biocompatible throughout the full Ag concentration range and a slight

improvement in cell viability could be observed for Ti rich and pure Ti samples following heat treatment, which could be related to an increase in crystallite size in these thin films.

This work has highlighted the potential of the $Ti_{(1-x)}Ag_{(x)}$ thin film system for application in load bearing biological settings. With further research a Ti-Ag coating containing ~43 at.% Ag could be successfully developed with high mechanical hardness, reduced wear rate and excellent biocompatibility to prolonging the lifetime of the next generation of medical devices and implants.

Acknowledgement
This work was funded and supported by a Leverhulme Trust Research Project Grant (RPG-2018-344) to develop super hard biocompatible coatings of a Ti based thin film material system.

Data Availability
The raw/processed data required to reproduce these findings cannot be shared at this time due to technical or time limitations.

References
[1] M. Abdel-Hady Gepreel, M. Niinomi, Biocompatibility of Ti-alloys for long-term implantation, J Mech Behav Biomed Mater, 20 (2013) 407-415.
[2] A. Etiemble, C. Lopes, G.I. Nkou Bouala, J. Borges, A. Malchère, C. Langlois, F. Vaz, P. Steyer, Fracture resistance of Ti-Ag thin films deposited on polymeric substrates for biosignal acquisition applications, Surface and Coatings Technology, 358 (2019) 646-653.
[3] C. Lopes, C. Gonçalves, J. Borges, T. Polcar, M.S. Rodrigues, N.P. Barradas, E. Alves, E. Le Bourhis, F.M. Couto, F. Macedo, C. Fonseca, F. Vaz, Evolution of the functional properties of titanium–silver thin films for biomedical applications: Influence of in-vacuum annealing, Surface and Coatings Technology, 261 (2015) 262-271.
[4] C. Lopes, P. Pedrosa, N. Martin, N.P. Barradas, E. Alves, F. Vaz, Study of the electrical behavior of nanostructured Ti–Ag thin films, prepared by Glancing Angle Deposition, Materials Letters, 157 (2015) 188-192.
[5] Y.L. Zhou, M. Niinomi, T. Akahori, H. Fukui, H. Toda, Corrosion resistance and biocompatibility of Ti–Ta alloys for biomedical applications, Materials Science and Engineering: A, 398 (2005) 28-36.
[6] C. Lopes, C. Gonçalves, P. Pedrosa, F. Macedo, E. Alves, N.P. Barradas, N. Martin, C. Fonseca, F. Vaz, TiAgx thin films for lower limb prosthesis pressure sensors: Effect of composition and structural changes on the electrical and thermal response of the films, Applied Surface Science, 285 (2013) 10-18.
[7] S. Ozan, J. Lin, Y. Li, R. Ipek, C. Wen, Development of Ti-Nb-Zr alloys with high elastic admissible strain for temporary orthopedic devices, Acta Biomater, 20 (2015) 176-187.
[8] J. Kesteven, M.B. Kannan, R. Walter, H. Khakbaz, H.C. Choe, Low elastic modulus Ti-Ta alloys for load-bearing permanent implants: enhancing the biodegradation resistance by electrochemical surface engineering, Mater Sci Eng C Mater Biol Appl, 46 (2015) 226-231.
[9] J.G. Yu, X.H. Sun, H.H. Gong, L. Dong, M.L. Zhao, R.X. Wan, H.Q. Gu, D.J. Li, Influence of Ag concentration on microstructure, mechanical properties and cytocompatibility of nanoscale Ti-Ag-N/Ag multilayers, Surface and Coatings Technology, 312 (2017) 128-133.
[10] C.T. Kao, S.J. Ding, Y.C. Chen, T.H. Huang, The anticorrosion ability of titanium nitride (TiN) plating on an orthodontic metal bracket and its biocompatibility, J Biomed Mater Res, 63 (2002) 786-792.
[11] J. Narayan, W.D. Fan, R.J. Narayan, P. Tiwari, H.H. Stadelmaier, Diamond, diamond-like and titanium nitride biocompatible coatings for human body parts, Materials Science and Engineering: B, 25 (1994) 5-10.
[12] R.A. Roşu, V.-A. Şerban, A.I. Bucur, U. Dragoş, Deposition of titanium nitride and hydroxyapatite-based biocompatible composite by reactive plasma spraying, Applied Surface Science, 258 (2012) 3871-3876.
[13] L. Torrisi, Ion implantation and thermal nitridation of biocompatible titanium, Bio-Medical Materials and Engineering, 6 (1996) 379-388.
[14] S. Dong, X. Chen, L. Gu, L. Zhang, X. Zhou, Z. Liu, P. Han, H. Xu, J. Yao, X. Zhang, L. Li, C. Shang, G. Cui, A biocompatible titanium nitride nanorods derived nanostructured electrode for biosensing and bioelectrochemical energy conversion, Biosens Bioelectron, 26 (2011) 4088-4094.

[15] M.P. Casaletto;, G.M.S. Kaciulis;, G. Mattogno;, L. Pandolfi;, G. Scavia, Surface studies of in vitro biocompatibility of titanium oxide coatings, Applied Surface Science, 172 (2001) 167-177.
[16] G.A. Crawford, N. Chawla, K. Das, S. Bose, A. Bandyopadhyay, Microstructure and deformation behavior of biocompatible TiO2 nanotubes on titanium substrate, Acta Biomater, 3 (2007) 359-367.
[17] C.-F. Huang, H.-C. Cheng, C.-M. Liu, C.-C. Chen, K.-L. Ou, Microstructure and phase transition of biocompatible titanium oxide film on titanium by plasma discharging, Journal of Alloys and Compounds, 476 (2009) 683-688.
[18] M.P. Casaletto, G.M. Ingo, S. Kaciulis, G. Mattogno, L. Pandolfi, G. Scavia, Surface studies of in vitro biocompatibility of titanium oxide coatings, Applied Surface Science, 172 (2001) 167-177.
[19] I. Kopova, J. Strasky, P. Harcuba, M. Landa, M. Janecek, L. Bacakova, Newly developed Ti-Nb-Zr-Ta-Si-Fe biomedical beta titanium alloys with increased strength and enhanced biocompatibility, Mater Sci Eng C Mater Biol Appl, 60 (2016) 230-238.
[20] C.-W. Chan, J. Quinn, I. Hussain, L. Carson, G.C. Smith, S. Lee, A promising laser nitriding method for the design of next generation orthopaedic implants: Cytotoxicity and antibacterial performance of titanium nitride (TiN) wear nano-particles, and enhanced wear properties of laser-nitrided Ti6Al4V surfaces, Surface and Coatings Technology, 405 (2021).
[21] H.N. Pantaroto, J.M. Cordeiro, L.T. Pereira, A.B. de Almeida, F.H. Nociti Junior, E.C. Rangel, N.F. Azevedo Neto, J.H.D. da Silva, V.A.R. Barao, Sputtered crystalline TiO2 film drives improved surface properties of titanium-based biomedical implants, Mater Sci Eng C Mater Biol Appl, 119 (2021) 111638.
[22] X.B. Tian, Z.M. Wang, S.Q. Yang, Z.J. Luo, R.K.Y. Fu, P.K. Chu, Antibacterial copper-containing titanium nitride films produced by dual magnetron sputtering, Surface and Coatings Technology, 201 (2007) 8606-8609.
[23] Y.L. Jeyachandran, S. Venkatachalam, B. Karunagaran, S.K. Narayandass, D. Mangalaraj, C.Y. Bao, C.L. Zhang, Bacterial adhesion studies on titanium, titanium nitride and modified hydroxyapatite thin films, Materials Science and Engineering: C, 27 (2007) 35-41.
[24] O. Akhavan, E. Ghaderi, Capping antibacterial Ag nanorods aligned on Ti interlayer by mesoporous TiO2 layer, Surface and Coatings Technology, 203 (2009) 3123-3128.
[25] S. Gurunathan, J.W. Han, D.-N. Kwon, J.-H. Kim, Enhanced antibacterial and anti-biofilm activities of silver nanoparticles against Gram-negative and Gram-positive bacteria, Nanoscale Research Letters, 9 (2014) 373.
[26] P. Pedrosa, D. Machado, P. Fiedler, B. Vasconcelos, E. Alves, N.P. Barradas, N. Martin, J. Haueisen, F. Vaz, C. Fonseca, Electrochemical characterization of nanostructured Ag:TiN thin films produced by glancing angle deposition on polyurethane substrates for bio-electrode applications, Journal of Electroanalytical Chemistry, 768 (2016) 110-120.
[27] M. Popović, M. Novaković, Z. Rakočević, N. Bibić, Tailoring the structural and optical properties of TiN thin films by Ag ion implantation, Nuclear Instruments and Methods in Physics Research Section B: Beam Interactions with Materials and Atoms, 389-390 (2016) 33-39.
[28] P. Pedrosa, E. Alves, N.P. Barradas, N. Martin, P. Fiedler, J. Haueisen, F. Vaz, C. Fonseca, Electrochemical behaviour of nanocomposite Agx:TiN thin films for dry biopotential electrodes, Electrochimica Acta, 125 (2014) 48-57.
[29] J. Zhao, H.J. Feng, H.Q. Tang, J.H. Zheng, Bactericidal and corrosive properties of silver implanted TiN thin films coated on AISI317 stainless steel, Surface and Coatings Technology, 201 (2007) 5676-5679.
[30] P. Pedrosa, C. Lopes, N. Martin, C. Fonseca, F. Vaz, Electrical characterization of Ag:TiN thin films produced by glancing angle deposition, Materials Letters, 115 (2014) 136-139.
[31] P. Pedrosa, D. Machado, C. Lopes, E. Alves, N.P. Barradas, N. Martin, F. Macedo, C. Fonseca, F. Vaz, Nanocomposite Ag:TiN thin films for dry biopotential electrodes, Applied Surface Science, 285 (2013) 40-48.
[32] J. Yu, J. Xiong, B. Cheng, S. Liu, Fabrication and characterization of Ag–TiO2 multiphase nanocomposite thin films with enhanced photocatalytic activity, Applied Catalysis B: Environmental, 60 (2005) 211-221.
[33] S. Sen, S. Mahanty, S. Roy, O. Heintz, S. Bourgeois, D. Chaumont, Investigation on sol–gel synthesized Ag-doped TiO2 cermet thin films, Thin Solid Films, 474 (2005) 245-249.
[34] O. Akhavan, E. Ghaderi, Self-accumulated Ag nanoparticles on mesoporous TiO2 thin film with high bactericidal activities, Surface and Coatings Technology, 204 (2010) 3676-3683.

[35] A.R. Malagutti, H.A.J.L. Mourão, J.R. Garbin, C. Ribeiro, Deposition of TiO2 and Ag:TiO2 thin films by the polymeric precursor method and their application in the photodegradation of textile dyes, Applied Catalysis B: Environmental, 90 (2009) 205-212.
[36] J. Zhou, Y. Cheng, J. Yu, Preparation and characterization of visible-light-driven plasmonic photocatalyst Ag/AgCl/TiO2 nanocomposite thin films, Journal of Photochemistry and Photobiology A: Chemistry, 223 (2011) 82-87.
[37] I.M. Arabatzis, T. Stergiopoulos, M.C. Bernard, D. Labou, S.G. Neophytides, P. Falaras, Silver-modified titanium dioxide thin films for efficient photodegradation of methyl orange, Applied Catalysis B: Environmental, 42 (2003) 187-201.
[38] M. Takahashi, M. Kikuchi, Y. Takada, Mechanical properties of dental Ti-Ag alloys with 22.5, 25, 27.5, and 30 mass% Ag, Dent Mater J, 34 (2015) 503-507.
[39] V. Kumar, S.K. Singh, H. Sharma, S. Kumar, M.K. Banerjee, A. Vij, Investigation of structural and optical properties of ZnO thin films of different thickness grown by pulsed laser deposition method, Physica B: Condensed Matter, 552 (2019) 221-226.
[40] W.C. Oliver, G.M. Pharr, An improved technique for determining hardness and elastic modulus using load and displacement sensing indentation experiments, Journal of Materials Research, 7 (1992) 1564-1583.
[41] M. Samuelsson, D. Lundin, J. Jensen, M.A. Raadu, J.T. Gudmundsson, U. Helmersson, On the film density using high power impulse magnetron sputtering, Surface and Coatings Technology, 205 (2010) 591-596.
[42] T.A. Kassam, A Review of the Alumina/Ag-Cu-Ti Active Metal Brazing Process, CRC Press2018.
[43] S. Liu, Y.C. Shin, Additive manufacturing of Ti6Al4V alloy: A review, Materials & Design, 164 (2019).
[44] A.A. Mosquera, J.M. Albella, V. Navarro, D. Bhattacharyya, J.L. Endrino, Effect of silver on the phase transition and wettability of titanium oxide films, Sci Rep, 6 (2016) 32171.
[45] T.H. Okabe, C. Zheng, Y.-k. Taninouchi, Thermodynamic Considerations of Direct Oxygen Removal from Titanium by Utilizing the Deoxidation Capability of Rare Earth Metals, Metallurgical and Materials Transactions B, 49 (2018) 1056-1066.
[46] K. Sun, J. Xue, K. Tai, S.J. Dillon, The Oxygen Reduction Reaction Rate of Metallic Nanoparticles during Catalyzed Oxidation, Sci Rep, 7 (2017) 7017.
[47] S. Ramanathan, Thin Film Metal-Oxides: Fundamentals and Applications in Electronics and Energy, Springer US2010.
[48] X. Wang, F. Prokert, H. Reuther, M.F. Maitz, F. Zhang, Chemical composition and biocompatibility of Ti–Ag–O films prepared by ion beam assisted deposition, Surface and Coatings Technology, 185 (2004) 12-17.
[49] F. Valenza, C. Artini, A. Passerone, M.L. Muolo, ZrB2–SiC/Ti6Al4V joints: wettability studies using Ag- and Cu-based braze alloys, Journal of Materials Science, 47 (2012) 8439-8449.
[50] V. Chawla, R. Jayaganthan, A.K. Chawla, R. Chandra, Microstructural characterizations of magnetron sputtered Ti films on glass substrate, Journal of Materials Processing Technology, 209 (2009) 3444-3451.
[51] H. Ju, L. Yu, D. Yu, I. Asempah, J. Xu, Microstructure, mechanical and tribological properties of TiN-Ag films deposited by reactive magnetron sputtering, Vacuum, 141 (2017) 82-88.
[52] D. Rajesh, C.S. Sunandana, XRD, optical and AFM studies on pristine and partially iodized Ag thin film, Results in Physics, 2 (2012) 22-25.
[53] R. Dimitrijevic, O. Cvetkovic, Z. Miodragovic, M. Simic, D. Manojlovic, V. Jovic, SEM/EDX and XRD characterization of silver nanocrystalline thin film prepared from organometallic solution precursor, Journal of Mining and Metallurgy, Section B: Metallurgy, 49 (2013) 91-95.
[54] P.H. Mayrhofer, C. Mitterer, L. Hultman, H. Clemens, Microstructural design of hard coatings, Progress in Materials Science, 51 (2006) 1032-1114.
[55] M.C. Jun, Y.S. Kim, M.K. Han, J.W. Kim, K.B. Kim, Polycrystalline silicon oxidation method improving surface roughness at the oxide/polycrystalline silicon interface, Applied Physics Letters, 66 (1995) 2206-2208.
[56] W.W. Gerberich, W.M. Mook, M.D. Chambers, M.J. Cordill, C.R. Perrey, C.B. Carter, R.E. Miller, W.A. Curtin, R. Mukherjee, S.L. Girshick, An Energy Balance Criterion for Nanoindentation-Induced Single and Multiple Dislocation Events, Journal of Applied Mechanics, 73 (2006) 327-334.

[57] Y. Wang, P.L. Tam, Y.G. Shen, Behavior of Ti0.5Al0.5N thin film in nanoscale deformation with different loading rates, Thin Solid Films, 516 (2008) 7641-7647.
[58] S.G. Corcoran, R.J. Colton, E.T. Lilleodden, W.W. Gerberich, Nanoindentation Studies of Yield Point Phenomena on Gold Single Crystals, MRS Online Proceedings Library, 436 (1996) 159-164.
[59] J. Ding, Y. Meng, S. Wen, Mechanical properties and fracture toughness of multilayer hard coatings using nanoindentation, Thin Solid Films, 371 (2000) 178-182.
[60] C.T. Chuang, C.K. Chao, R.C. Chang, K.Y. Chu, Effects of internal stresses on the mechanical properties of deposition thin films, Journal of Materials Processing Technology, 201 (2008) 770-774.
[61] A.K. Nanda Kumar, C.K. Sasidharan Nair, M.D. Kannan, S. Jayakumar, TEM and nanoindentation studies on sputtered Ti40Ni60 thin films, Materials Chemistry and Physics, 97 (2006) 308-314.
[62] W.-G. Jiang, J.-J. Su, X.-Q. Feng, Effect of surface roughness on nanoindentation test of thin films, Engineering Fracture Mechanics, 75 (2008) 4965-4972.
[63] L. Chen, A. Ahadi, J. Zhou, J.-E. Ståhl, Modeling Effect of Surface Roughness on Nanoindentation Tests, Procedia CIRP, 8 (2013) 334-339.
[64] N.G. Demas, C. Lorenzo-Martin, O.O. Ajayi, R.A. Erck, I. Shareef, Measurement of Thin-film Coating Hardness in the Presence of Contamination and Roughness: Implications for Tribology, Metallurgical and Materials Transactions A, 47 (2016) 1629-1640.
[65] C. Walter, T. Antretter, R. Daniel, C. Mitterer, Finite element simulation of the effect of surface roughness on nanoindentation of thin films with spherical indenters, Surface and Coatings Technology, 202 (2007) 1103-1107.
[66] Y.X. Leng, J.Y. Chen, P. Yang, H. Sun, N. Huang, Structure and properties of passivating titanium oxide films fabricated by DC plasma oxidation, Surface and Coatings Technology, 166 (2003) 176-182.
[67] P. Larsson, H. Engqvist, J. Biermann, E. Werner Ronnerman, E. Forssell-Aronsson, A. Kovacs, P. Karlsson, K. Helou, T.Z. Parris, Optimization of cell viability assays to improve replicability and reproducibility of cancer drug sensitivity screens, Sci Rep, 10 (2020) 5798.
[68] A.A. Stepanenko, V.V. Dmitrenko, Pitfalls of the MTT assay: Direct and off-target effects of inhibitors can result in over/underestimation of cell viability, Gene, 574 (2015) 193-203.
[69] S. Mateti, C.S. Wong, Z. Liu, W. Yang, Y. Li, L.H. Li, Y. Chen, Biocompatibility of boron nitride nanosheets, Nano Research, 11 (2017) 334-342.
[70] M. Chen, L. Yang, L. Zhang, Y. Han, Z. Lu, G. Qin, E. Zhang, Effect of nano/micro-Ag compound particles on the bio-corrosion, antibacterial properties and cell biocompatibility of Ti-Ag alloys, Mater Sci Eng C Mater Biol Appl, 75 (2017) 906-917.
[71] K. Jamuna-Thevi, S.A. Bakar, S. Ibrahim, N. Shahab, M.R.M. Toff, Quantification of silver ion release, in vitro cytotoxicity and antibacterial properties of nanostuctured Ag doped TiO2 coatings on stainless steel deposited by RF magnetron sputtering, Vacuum, 86 (2011) 235-241.
[72] E.P. Ivanova, J. Hasan, V.K. Truong, J.Y. Wang, M. Raveggi, C. Fluke, R.J. Crawford, The influence of nanoscopically thin silver films on bacterial viability and attachment, Appl Microbiol Biotechnol, 91 (2011) 1149-1157.
[73] S. Rashid, G.M. Vita, L. Persichetti, G. Iucci, C. Battocchio, R. Daniel, D. Visaggio, M. Marsotto, P. Visca, E. Bemporad, P. Ascenzi, G. Capellini, M. Sebastiani, A. di Masi, Biocompatibility and antibacterial properties of TiCu(Ag) thin films produced by physical vapor deposition magnetron sputtering, Applied Surface Science, 573 (2022).
[74] S. Rashid, M. Sebastiani, M.Z. Mughal, R. Daniel, E. Bemporad, Influence of the Silver Content on Mechanical Properties of Ti-Cu-Ag Thin Films, Nanomaterials (Basel), 11 (2021).
[75] D. Gospodonova, I. Ivanova, T. Vladkova, Fabrication and Characterization of Antimicrobial Magnetron Cosputtered TiO2/Ag/Cu Composite Coatings, Coatings, 11 (2021).